Atmospheric Environment 147 (2016) 79–87

Contents lists available at ScienceDirect

Atmospheric Environment

journal homepage: www.elsevier.com/locate/atmosenv

Hydrogen shift reactions in four methyl-buten-ol (MBO) peroxy radicals and their impact on the atmosphere

Hasse C. Knap, Johan A. Schmidt, Solvejg Jørgensen*

Department of Chemistry, University of Copenhagen, Universitetsparken 5, 2100 Copenhagen Ø, Denmark

HIGHLIGHTS

- An investigation of the impact of the H-shift reactions in the oxidation of MBO232.
- The rate constants for the atmospheric decomposition are implemented in GEOS-Chem.
- H-shift reactions in the MBO232 peroxy radical play a minor role.
- Glycolaldehyde is a major decomposition compound from the MBO232 oxidation.
- Epoxides are most likely not formed after H-shift reaction in the oxidation of MBO232.

GRAPHICAL ABSTRACT

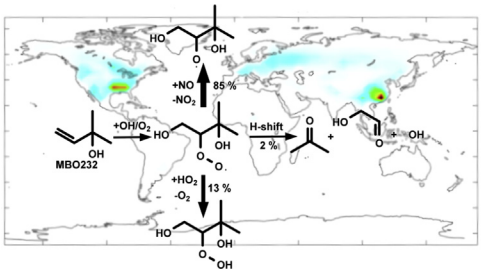

ARTICLE INFO

Article history:
Received 27 May 2016
Received in revised form
13 September 2016
Accepted 27 September 2016
Available online 28 September 2016

Keywords:
2-Methyl-3-buten-2-Ol
Peroxy radical
Hydrogen shift
Atmospheric impact
GEOS-Chem

ABSTRACT

We investigate the hydrogen shift (H-shift) reactions in the peroxy radicals derived from four different methyl-buten-ol (MBO) molecules; 2-methyl-3-buten-2-ol (MBO232), 2-methyl-3-buten-1-ol (MBO231), 3-Methyl-3-buten-2-ol (MBO332) and 3-methyl-3-buten-1-ol (MBO331), with quantum mechanical calculations. The rate constants of the 1,5 H-shift reactions in all four MBO peroxy radicals are greater than the rate constants of the 1,4 or 1,6 H-shift reactions. The rate constants for the 1,5 H-shift reaction from either a CH group or an OH group are approximately 1 s^{-1} and 10^{-3} s^{-1}, respectively. The atmospheric impact of the MBO232 oxidation is investigated with the global chemical transport model (GEOS-Chem). The 1,4-CH and 1,5-OH H-shift reactions in the MBO232 peroxy radical play a minor role with a total yield of about 2%. The major atmospheric reactions of the MBO232 peroxy radical are the reactions with NO and HO_2, with reaction yield of 85% and 13%, respectively.

1. Introduction

Methyl-buten-ol (MBO) molecules are emitted from many different natural sources (Baker et al., 1999; Goldan et al., 1993; Harley et al., 1998; Koenig et al., 1995). The most important biogenic emitted MBO is the 2-methyl-3-buten-2-ol (MBO232) with an estimated global emission around 1.6–2.2 Tg yr^{-1} (Guenther et al., 2012; Sindelarova et al., 2014). Although the global emission of MBO232 is 200–400 times lower than the emission of isoprene (500–600 Tg yr^{-1}) (Guenther et al., 2012; Sindelarova et al., 2014), the local concentration of MBO232 can exceed the concentration of isoprene in some regions. In the Colorado Mountains the daytime mixing ratio of MBO232 is measured to be 2–3 ppb, which is about 4–7 times greater than the concentration of isoprene (0.4–0.6 ppb) (Goldan et al., 1993).

* Corresponding author.
E-mail address: solvejg@chem.ku.dk (S. Jørgensen).

http://dx.doi.org/10.1016/j.atmosenv.2016.09.064
1352-2310/

The oxidation of MBO232 in the atmosphere is initiated by the reaction with the hydroxyl (OH) radical. This reaction has been investigated both experimentally and theoretically (Alvarado et al., 1999; Baasandorj and Stevens, 2007; Carrasco et al., 2007; Chan et al., 2009; Fantechi et al., 1998; Ferronato et al., 1998; Reisen et al., 2003). The rate constant for MBO232 + OH is measured to 6.3×10^{-11}cm^3 molecules^{-1} s^{-1} (Baasandorj and Stevens, 2007). Here the OH radical adds to the double bond in MBO232, where the addition occurs at the terminal carbon atom with a probability of 0.7 (Alvarado et al., 1999; Baasandorj and Stevens, 2007). The subsequent addition of molecular oxygen produces a peroxy radical (MBO232-RO_2). The oxidation of MBO232 produces secondary organic aerosols (SOA), when the NO concentration is low (Chan et al., 2009; Jaoui et al., 2012; Zhang et al., 2012). It is proposed, that the possible formation of the SOA is due to the production of C_5-triols, by a self-reaction between two MBO232-RO_2 radicals (Chan et al., 2009). Recently, it is suggested, that an internal hydrogen transfer reaction (H-shift) from an alcohol group could lead to the formation of epoxides (Zhang et al., 2014). Current results suggest that epoxides might be an important SOA precursor, which could contribute to SOA production in forest regions (Paulot et al., 2009; St. Clair et al., 2016; Zhang et al., 2012, 2014).

In general, peroxy radicals (RO_2) can self-react (RO_2 + RO_2), react with NO/HO_2, or undergo an internal transfer of a hydrogen atom (H-shift reaction). If the H-shift reaction is fast and/or if the concentration of NO/HO_2 is low, like in remote forest regions, the H-shift reactions become important for RO_2. The rate constants of the pseudo-first order reaction between RO_2 and NO/HO_2 are estimated to be around 10^{-2} s^{-1} in remote forest regions with ambient temperature and pressure (Orlando and Tyndall, 2012). In H-shift reactions, RO_2 transfers a hydrogen atom internally and produces a QOOH radical. The QOOH radical can hereafter decompose into smaller molecules, or react with O_2 and produce a new peroxy (OOQOOH) radical. The OOQOOH radicals can then again undergo a H-shift reactions or reacts with NO or HO_2. This process is known as autoxidation (Crounse et al., 2013).

RO_2 can undergo a number of unimolecular decomposition reactions (predominantly, internal transfer of a hydrogen atom). The H-shift reaction of an aldehydic hydrogen atom has been shown to be important in the atmosphere with a rate constant of around 0.5 s^{-1} (Crounse et al., 2012). Very recently, the H-shift reaction from a hydroperoxy group and an enol have been estimated to be very fast with rate constants of about 10^3 s^{-1} and 10^6 s^{-1}, respectively (Jørgensen et al., 2016; Peeters and Nguyen, 2012). The H-shift autoxidation mechanism has been shown to produce extremely low-volatility organic compounds (ELVOCs) by introducing a large amount of hydroperoxy groups into the VOCs (Rissanen et al., 2014). In the oxidation of isoprene, H-shift reactions will compete with the bimolecular reaction of RO_2 with NO/HO_2 (Crounse et al., 2011; Peeters et al., 2009). There are six different isoprene derived peroxy radicals. Two of the isoprene derived peroxy radicals, $HOCH_2CHC(CH_3)CH_2(OO)$ and $HOCH_2C(CH_3)CHCH_2(OO)$, can undergo a 1,6-CH H-shift reaction leading to the production of C_5-hydroperoxyaldehydes (HPALDs) (Peeters et al., 2009), whereas the four other isoprene derived peroxy radicals, $(HOCH_2C(CH_3)(OO)CHCH_2$, $(OO)CH_2C(CH_3)(OH)CHCH_2$, $HOCH_2CH(OO)C(CH_3)CH_2$ and $(OO)CH_2CH(OH)C(CH_3)CH_2)$, can undergo a 1,5-OH H-shift reaction. The rate constants of the 1,5-OH H-shift reactions are estimated to be in the range 10^{-4}-10^{-2} s^{-1} at 300 K (Da Silva et al., 2010; Peeters et al., 2009, 2014).

Here, we will investigate the possible H-shift reactions in peroxy radicals derived from the OH radical oxidation of four different MBOs (2-methyl-3-buten-2-ol (MBO232), 2-methyl-3-buten-1-ol (MBO231), 3-methyl-3-buten-2-ol (MBO332) and 3-methyl-3-buten-1-ol (MBO331)). The position of the methyl group, carbon-carbon double bond and alcohol group are the first, second and third number, respectively. The molecular structures are shown in Fig. 1. We will also investigate a possible reaction mechanism for the formation of epoxides from the peroxy radicals derived from MBO232. Furthermore, we will simulate the atmospheric impact of the OH radical oxidation of MBO232, using the GEOS-Chem chemical transport model (Bey et al., 2001) and employing the MEGAN 2.1 emission inventory (Guenther et al., 2012).

2. Computational details

2.1. Ab initio calculations

Initially, we optimize all transition states (TS) using the B3LYP/6-31+G(d,p) method (Becke, 1988, 1993; Frisch et al., 1984; Lee et al., 1988). Intrinsic reaction coordinate (IRC) calculations are preformed in order to ensure that the TS is connected to the desired reactant and product (Gonzalez and Schlegel, 1989, 1990). We calculate the IRC with 50 points in each direction with default step size. The reactant and product are found by an optimization of the endpoint of the IRC. Subsequently, the structures are optimized with the M06-2X/aug-cc-pVTZ method (Dunning, 1989; Zhao and Truhlar, 2008). The forward and reverse rate constants calculated from these structures are denoted $k_{IRC\text{-}TST}$ and is calculated by the transition state theory and corrected with the one dimensional Eckart quantum tunneling coefficient. The M06-2X/aug-cc-pVTZ method calculates energy barrier heights for H-shift reactions which are in good agreement with the ones obtained with single-point CCSD(T)-F12A/VDZ-F12 (Knap et al., 2015).

A full conformer search is performed on all the possible 1,5 H-shift reactions in the MBO peroxy radicals in order to find the conformers with the lowest zero-point corrected energy. We use the M06-2X/aug-cc-pVTZ optimized structures as an initial guess structure for the reactant, TS and product in the conformer search. The conformer search is performed as described in the following five steps: i) An initial set of conformers (reactant, transition state and product) are generated by the Sybyl force field method in the Spartan program (Spartan'10, 2010). ii) For all of the generated conformers a single-point B3LYP/6-31+G(d) energy is calculated. We order all the conformers with respect to the single-point B3LYP/6-31+G(d) electronic energies. We select all the conformers with the energy up to 10 kcal/mol higher than the conformer with the lowest single-point B3LYP/6-31+G(d) electronic energy. iii) The

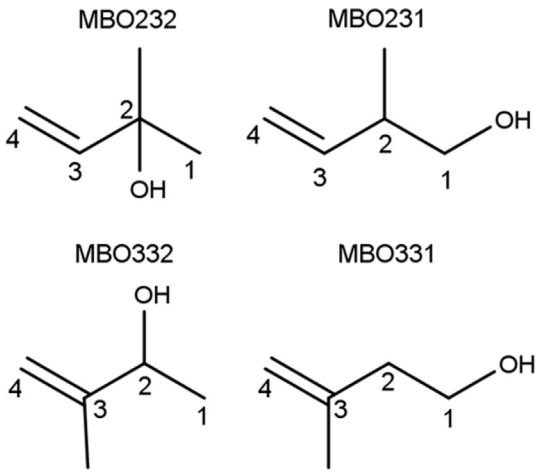

Fig. 1. The four different methyl-buten-ols (MBO) are shown with labeled carbon atoms. Top left is the 2-methyl-3-buten-2-ol, top right the 2-methyl-3-buten-1-ol, bottom left 3-methyl-3-buten-2-ol and bottom right is the 3-methyl-3-buten-1-ol.

selected conformers are optimized and vibrational frequencies are calculated with the B3LYP/6-31+G(d,p) method using the Gaussian 09 program (Frisch et al., 2009). After the B3LYP/6-31+G(d,p) optimization we order the conformer with respect to zero-point corrected energy. We select the conformers with the energy up to 2 kcal/mol higher than the conformer with the lowest B3LYP/6-31+G(d,p) zero-point corrected energy. iv) The selected conformers are optimized and vibrational frequencies are calculated with the M06-2X/aug-cc-pVTZ method. We order the M06-2X/aug-cc-pVTZ optimized conformers with respect to zero-point corrected energies. We select the conformer with the lowest zero-point corrected M06-2X/aug-cc-pVTZ energy for further investigation. v) Finally, we calculate a single-point ROHF-UCCSD(T)-F12A/VDZ-F12 (Adler et al., 2007; Peterson et al., 2008) (F12) energy on the lowest M06-2X/aug-cc-pVTZ zero-point corrected energy conformer. The F12 energies are calculated with the Molpro2012 program (Werner et al., 2012a, 2012b) using default convergence criteria but the germinal Slater coefficient is set to 0.9 and the F12 triplet contribution was scaled (Marchetti and Werner, 2009; Peterson et al., 2008). The CCSD(T)-F12A/VDZ-F12 energies have been shown to be comparable to CCSD(T)/aug-cc-pVQZ energies (Lane and Kjaergaard, 2009). We summarize the numbers of conformers in each of the above steps in the supplemental material (Table A.5-A.8).

The open-shell structures calculated with the B3LYP/6-31+G(d,p) and M06-2X/aug-cc-pVTZ methods are checked for spin contamination, both before and after the spin annihilation. We observed no spin contamination in any of our structures. The T_1-diagnostic values in the F12 calculations are also evaluated, a high T_1-diagnostic value indicate that multi-reference character might be present in the F12 wave function. For all four MBO-RO_2 radicals, the transition state structures of the 1,5-OH H-shift reactions have T_1-diagnostic values above 0.06. High T_1-diagnostic values have been observed and reported before for similar alcoholic H-shift reactions in peroxy radicals and a CI coefficient analysis from multi-reference method calculations (CASSCF) showed that a single-reference should be an acceptable representation for the electronic wave function for alcoholic H-shift reactions in peroxy radicals (Knap et al., 2015; Peeters and Nguyen, 2012). We have reported the M06-2X/aug-cc-pVTZ energies, since the 1,5-OH H-shift reactions have high T_1-diagnostic values. The M06-2X/aug-cc-pVTZ total spin and F12 T_1-diagnostic values are shown in the supplemental material. The M06-2X/aug-cc-pVTZ method has been shown to estimate barrier heights and imaginary frequencies for similar H-shift reactions with an accuracy close to that of the F12 methods (Knap et al., 2015).

2.2. Transition state rate constant

We use transition state theory (TST) to calculate rate constants of all the forward and reverse H-shift reactions (Holbrook et al., 1996)

$$k_{TST} = \kappa \frac{k_b T}{h} \frac{Q_{TS}}{Q_R} \exp\left(- \frac{E_{TS} - E_R}{k_b T} \right) \quad (1)$$

where E_{TS} and E_R are the zero-point corrected energy of the lowest conformer for the TS and reactant, respectively. The constants, h and k_b, are the Planck and the Boltzmann constant, respectively. The temperature, T, is set to 298.15 K. Q_{TS} and Q_R are the partition functions of the transition state and reactant, respectively. The rigid rotor and the harmonic oscillator approximations are used to calculate the rotational and vibrational partition functions, respectively. All of the partition functions are calculated based on the M06-2X/aug-cc-pVTZ structures and vibrational frequencies. The rate constants calculated with the lowest conformers of the reactant, transition state and product is denoted k_{TST}. Quantum tunneling, κ, is estimated with the one dimensional Eckart quantum tunneling correction (Eckart, 1930). For the H-shift reactions in the n-propylperoxy radical, the one dimensional Eckart quantum tunneling correction has been shown to predict tunneling corrections in good agreement with small curvature tunneling (SCT) correction (Zhang and Dibble, 2011).

We have not included hindered rotational effects in the rate constants of H-shift reactions. In the autoxidation of the cyclohexene, the inclusion of the hindered rotor effects decreases the forward (reverse) rate constant of the H-shift reactions with less than a factor of 6 compared to forward (reverse) rate constants of the H-shifts without including hindered rotor effects (Rissanen et al., 2014).

2.3. MESMER simulations

We use the Master Equation Solver for Multi Energy-well Reactions (MESMER) program (Glowacki et al., 2012) to calculate the overall rate constants (k_M) of the MBO232 peroxy radical (MBO232-RO_2) resulting from the oxidation of the MBO232 by OH (+O_2) at ambient atmospheric conditions.

The initial reaction of MBO232 with the OH radical produce the MBO232-OH adduct with an exothermic energy, hence we have include an excess energy to the MBO232-OH adduct in our MESMER simulation. For the reaction between MBO232-OH and the O_2 radical leading to MBO232-RO_2, we use an Arrhenius pre-exponential factor (A) of 3.0×10^{-12} cm^3 molecules^{-1} s^{-1} and $[O_2] = 5.2 \times 10^{18}$ molecules cm^{-3} (Park et al., 2004). We use the MesmerITL method for the reaction MBO232-RO_2 → MBO232-OH + O_2. For the irreversible bimolecular reaction between the 14QOOH radical with O_2 the SimpleBimolecularSink method is used with a rate constant of $k_{O2} = 3.0 \times 10^{-12}$ cm^3 molecules^{-1} s^{-1} and an $[O_2] = 5.2 \times 10^{18}$ molecules cm^{-3} (Park et al., 2004). The SimpleRRKM method is used for all the other reactions and the Eckart quantum tunneling correction is applied on all of the H-shift reactions.

The default collision energy transfer model (e.i. the exponential down model) is used. For all modeled species along the reaction path we use $\Delta E_{down} = 200$ cm^{-1}. All the involved structures are very similar with respect to size and mass; therefore we use the same Lennard-Jones (L-J) parameter for all of the structures, which we assume to be $\sigma = 7.045$ Å and $\varepsilon = 379.95$ K for the methylcyclohexane molecule, which has a similar size as our modeled species (Cuadros et al., 1996). The L-J parameters for the bath gas (N_2) are set to $\sigma = 3.919$ Å and $\varepsilon = 91.85$ K (Cuadros et al., 1996). In all the MESMER simulations, the pressure, temperature and grain size are 1 atm, 298.15 K and 100 cm^{-1}, respectively. The bath-gas mean collision frequency is about 1.6×10^{10} s^{-1} in all of our MESMER simulations. The default maximum integration time is used. Furthermore, we use the automatic algorithm to specify the energy range of the grain span.

We perform a sensitivity analysis on the grain size, the L-J parameters, ΔE_{down} and the number precision. The sensitivity analysis is discussed in the supplemental material.

2.4. GEOS-Chem simulation

We use the GEOS-Chem global chemical transport model (v10-01) (Bey et al., 2001) including a detailed ozone-HOx-NOx-VOC-aerosol-Br tropospheric chemistry mechanism. The model is driven by GEOS-5 assimilated meteorological data from the NASA Global Modeling and Assimilation Office with $1/2 \times 2/3^\circ$ horizontal resolution and 47 vertical layers extending up to approximately

80 km. The horizontal resolution is degraded to 4 × 5° for input to GEOS-Chem. The time step for transport is 30 min and the time steps for chemistry and emission are 60 min. The simulation was then run for a full year using 2007 as the model year. The output from this run was used in the analysis.

The emission of MBO232 is implemented using archived monthly emissions from the Model of Emissions of Gases and Aerosols from Nature version 2.1 (MEGAN 2.1 emission inventory) modeling framework (Guenther et al., 2012). The chemistry mechanism of GEOS-Chem is extended including MBO232 and 6 intermediates and products. The MBO chemistry mechanism is summarized in Figure A.8 in the supplemental material.

3. Results and discussion

3.1. H-shift reactions in the four MBO peroxy radicals

We investigate the atmospheric oxidation by the OH radical of four MBOs, MBO232, MBO231, MBO331, and MBO332. The addition of the OH radical to the outer carbon atom (C4) in the carbon double bond of MBO232 (CH_2=$CHCOH(CH_3)CH_3$) has been shown to be the most dominant reaction path with a probability of 0.7 (Alvarado et al., 1999; Baasandorj and Stevens, 2007). Subsequently, molecular oxygen (O_2) adds to the inner carbon atom (C3) and MBO232-RO_2 ($HOCH_2CH(OO)C(OH)(CH_3)CH_3$) is formed. Since all four MBOs have the double bond between C3 and C4, we assume that all of the MBOs produce a peroxy radical (RO_2) similar to MBO232-RO_2. The produced peroxy radicals (RO_2) will be denoted as MBO232-RO_2, MBO231-RO_2, MBO331-RO_2 and MBO332-RO_2 for each of the four MBOs. RO_2 can undergo H-shift reactions, self-react, or react with NO or HO_2. We have earlier studied the H-shift reactions of MBO331-RO_2 (Knap et al., 2015).

Here, the reported rate constants ($k_{IRC-TST}$) are not necessarily for the conformer with the lowest zero-point corrected energy, since the conformers are found from the endpoint of the IRC. The reaction scheme for MBO232-RO_2 is shown in Fig. 2 (Figure A.1-A.3 in the supplemental material show the reaction scheme of MBO231-RO_2, MBO331-RO_2 and MBO332-RO_2, respectively).

The rate constants ($k_{IRC-TST}$) for the forward H-shift reaction in all four MBO-RO_2 are in the order 1,5-CH > 1,5-OH > 1,6-OH ≈ 1,4-CH, whereas the rate constants for the reverse H-shift reaction are in the order 1,5-OH > 1,6-OH > 1,5-CH > 1,4-CH. The 1,4-CH H-shift reactions are known to have a slow rate constant due to the ring strain of the transition state, this is in good agreement with our observations. For all four MBO-RO_2 the 1,5 H-shift reactions are the fastest H-shift reaction, therefore we will only do a full conformer search on these reactions.

In Table 1 are the rate constants (k_{TST}) calculated from the lowest conformer of the reactant, transition state, and product with the zero-point corrected M06-2X/aug-cc-pVTZ energy. The barrier heights and rate constants (k_{TST}) for the forward and reverse 1,5 H-shift reactions for all MBO-RO_2 are shown in Table 1, with the M06-2X/aug-cc-pVTZ method. (The F12//M06-2X/aug-cc-pVTZ calculated energies and the rate constants are shown in Table A.9 in the supplemental material.)

In general, we observe, that the conformers of the reactant, transition state, and product with the lowest zero-point corrected M06-2X/aug-cc-pVTZ energy have one or two hydrogen bonds. MBO331-RO_2 and MBO231-RO_2 can both undergo a 1,5-CH H-shift reaction. The rate constants (k_{TST}) for the two forward 1,5-CH H-shift reactions are about 1 s^{-1}, whereas the rate constants for the reverse reaction are about 10^5 s^{-1}. The forward and reverse F12//M06-2X/aug-cc-pVTZ calculated rate constants (k_{TST}) for the two 1,5-CH H-shift reactions are 3–20 times faster than the M06-2X/aug-cc-pVTZ calculated rate constants (k_{TST}). All four MBO-RO_2 can undergo 1,5-OH H-shift reactions, the rate constants (k_{TST}) for the forward 1,5-OH H-shift are between 10^{-4}-10^{-3} s^{-1}, whereas the reverse H-shift reactions are very fast with rate constants (k_{TST}) around 10^{10}-10^{11} s^{-1}. The major reason for the differences in the forward and reverse rate constants (k_{TST}) for a 1,5-OH H-shift reaction is the differences in the barrier heights.

MBO231-RO_2 and MBO232-RO_2 are both secondary peroxy radicals, whereas MBO331-RO_2 and MBO332-RO_2 are tertiary peroxy radicals. Both the barrier heights for the 1,5-OH and 1,5-CH H-shift reactions in the two tertiary MBO-RO_2 are similar to ones for the 1,5-OH and 1,5-CH H-shift reactions in the secondary MBO-RO_2 (MBO231-RO_2 versus MBO331-RO_2 and MBO232-RO_2 versus MBO332-RO_2). Whether RO_2 is a secondary or tertiary peroxy radical, we only observe a minor effect on the rate constants (k_{TST}) for the H-shift reactions. The same trend is observed for the H-shift reactions in the isoprene derived peroxy radicals (Da Silva et al., 2010). The rate constants for the 1,5a-OH H-shift reaction in MBO232-RO_2 and MBO332-RO_2 are 5–10 times greater than the rate constants (k_{TST}) for the 1,5-OH H-shift reaction in MBO231-RO_2 and MBO331-RO_2. The position of the second alcohol group at the C2 (compared to C1) carbon atom lowers the rate constant (k_{TST}) of the forward 1,5a-OH reaction, whereas the position of the alcohol group on either C1 or C2 has no significant effect on the rate constant (k_{TST}) of the reverse 1,5-OH H-shift reactions.

The rate constants for the 1,5-OH H-shift reactions in two of the six isoprene derived peroxy radicals ($HOCH_2C(CH_3)(OO)CHCH_2$ and $CH_2C(CH_3)CH(OO)CH_2OH$) are calculated to be about 10^{-4} s^{-1} with the CBS-QB3 method (Da Silva et al., 2010; Peeters et al., 2009), and latter refined to be around 10^{-3} s^{-1} with the high level method (CCSD(T)/aug-cc-pVTZ//QCISD/6-311G (d,p)) (Peeters et al., 2014). All rate constants are within the same magnitude as our calculated rate constants (k_{TST}) for the 1,5-OH H-shift reaction in all four MBO-RO_2. The presence of the carbon double bond in the isoprene derived peroxy radicals versus the absence of the double carbon bond in MBO-RO_2 has a minor effect on the rate constant (k_{TST}) for the forward 1,5-OH H-shift. The 1,5-OH H-shift reactions in the isoprene derived peroxy radicals are irreversible, since the products of the 1,5-OH H-shift reactions decompose without an energy barrier (Da Silva et al., 2010; Peeters et al., 2009). We observe, that the decomposition reaction for the product formed in the 1,5-OH H-shift in MBO232-RO_2 has a barrier above 3 kcal/mol (see Table A.10 in the supplemental material), this show that the reverse 1,5-OH H-shift in MBO-RO_2 may be of importance.

3.2. Hydrogen shift reactions in the 2-methyl-3-buten-2-ol peroxy radical

MBO232 is a well known biogenic emitted MBO, with a global emission around 1.6–2.2 Tg yr^{-1} (Guenther et al., 2012; Sindelarova et al., 2014). MBO331 is a naturally emitted MBO but with very low emission rates (Koenig et al., 1995), whereas MBO231 and MBO332 to our knowledge are not naturally emitted. Therefore, we only focus on the atmospheric decomposition of MBO232. The atmospheric decomposition reaction scheme of MBO232 is shown in Fig. 2 and its energy diagram is shown in Fig. 3 (see also Table A.11 in the supplemental material for the energies). MBO232-RO_2 can undergo three different H-shift reactions (1,5a-OH, 1,5b-OH, and 1,4-CH).

After the 1,5-OH H-shift reactions an alkoxy radical (QOOH) is produced. The 15aQOOH radical, produced after the 1,5a-OH H-shift reaction, undergoes α-scission reaction where the bond between C3-C4 breaks, whereas after the 1,5b-OH H-shift reaction the 15bQOOH radical can break the C2-C3 bond also called β-scission. The two scission reactions produce an unstable α-OOH alkyl radical, which decomposes into an OH radical and an aldehyde molecule

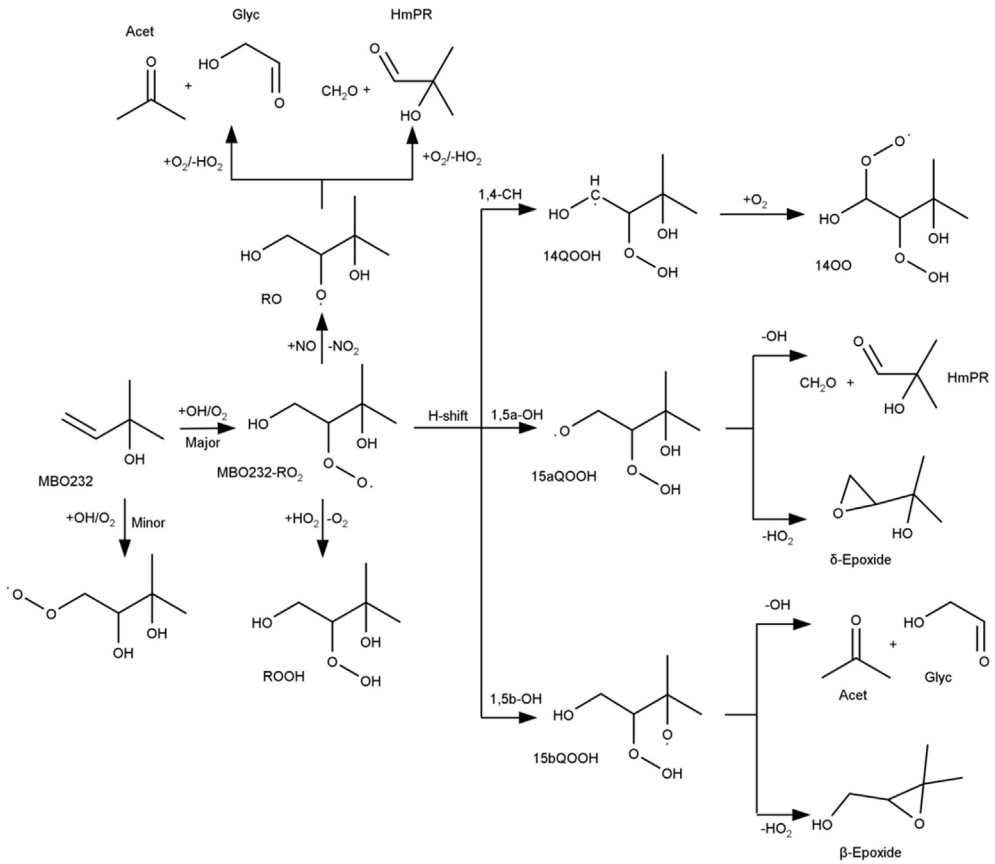

Fig. 2. The reaction scheme of the atmospheric decomposition of MBO232.

(Vereecken et al., 2004). The overall products after the 1,5a-OH H-shift and α-scission reactions are an OH radical, 2-hydroxy-2-methyl-propanal (HmPR), and formaldehyde (CH_2O), whereas glycolaldehyde (Glyc), acetone (Acet), and an OH radical, are produced after the 1,5b-OH H-shift and β-scission reactions.

Recently, it has been suggested, that the 15aQOOH and 15bQOOH radicals could undergo a rearrangement to form an epoxide and HO_2 (Zhang et al., 2014). In the suggested reaction mechanism the alkoxy group in the 15aQOOH and 15bQOOH radicals makes a bond with the carbon atom where the OOH group is attached. In the optimized transition state structure, the epoxide formation is a single step reaction mechanism, where HO_2 leaves in the same motion as the epoxide is produced. The 15aQOOH and 15bQOOH radicals can produce a δ-epoxide and β-epoxide, respectively. The barrier heights for the formation reaction of the two epoxides are very high (above 30 kcal/mol) compared to the two scission reactions (less than 8 kcal/mol). Furthermore, we also found that the energy of the products, epoxide and HO_2, are about 8 kcal/mol above the energy of the QOOH radical. Hence, we conclude that the epoxide formation is unlikely through the 1,5-OH H-shift reaction pathways.

After the 1,4-CH H-shift reaction in MBO232-RO_2, the 14QOOH radical can react with O_2 or make a reverse 1,4-CH H-shift reaction. The reverse 1,4-CH H-shift reaction is significantly slower ($<10^6$ times) than the pseudo-first order rate constant for the reaction between the 14QOOH radical and O_2 leading to the 14OO radical. Subsequently, the 14OO radical can undergo different H-shift reactions or react with NO/HO_2. The decompositions reactions of the 14OO radical are shown in Figure A.4 in the supplemental material.

In our MESMER simulation the 1,4-CH reaction is stopped after the 14OO radical is produced e.g. the 14OO radical is assumed to be the sink. The MESMER calculated yields and overall rate constants (k_M) of our decomposition of MBO232-RO_2 are shown in Table 2. The overall rate constant (k_M) of the 1,5b-OH H-shift reaction and subsequent β-scission in Table 2 is a factor of 10 slower than the forward 1,5b-OH H-shift reaction rate constant (k_{TST}) in Table 1. The overall rate constants (k_M) calculated in the MESMER simulations are the overall rate constant from MBO232-RO_2 to the products, whereas the k_{TST} is only the rate constant for the forward 1,5b-OH H-shift reaction leading to the 15bQOOH radical. The overall rate constant (k_M) is slower than the forward 1,5b-OH H-shift reaction rate constant (k_{TST}) due to the fact that barrier height of the reverse H-shift reaction is 2.2 kcal/mol whereas the barrier height of the subsequent β-scission is 3.2 kcal/mol (see Table A.11). The overall rate constants (k_M) are in the order of $k_{Acet+Glyc} \approx k_{14OO} > k_{HmPR+CH2O} >> k_{\beta\text{-}Epoxide} \approx k_{\delta\text{-}Epoxide}$. We have tested the sensitivity of the barrier height by either increasing or decreasing the barrier heights by 1 kcal/mol, see Table A.13-A.14 in the supplemental material. The effect of either increasing or decreasing the barrier heights are about a factor of 5 on all of the overall rate constants (k_M). If we include the uncertainty of the overall rate constant then the overall rate constant through the 1,5b-OH H-shift becomes equivalent to the pseudo-first order rate constants when NO and HO_2 concentrations are between 0.2-5 ppt and 0.1-3 ppt, respectively. We have used the bimolecular rate constants; $k_{NO} = 9.0 \times 10^{-12}$ cm^3 $molecules^{-1}$ s^{-1} and $k_{HO2} = 1.7 \times 10^{-11}$ cm^3 $molecules^{-1}$ s^{-1}, (Boyd et al., 2003; Park et al., 2004).

Most of the MBO232-RO_2 have enough internal energy to promptly (within 10^{-6} s) overcome the first H-shift barrier height

Table 1
The M06-2X/aug-cc-pVTZ calculated parameters for the 1,5 H-shift reactions in the four MBO-RO_2.

MBO-RO_2	Transition state	H-shift	E_F[a]	E_R[b]	k_F[c]	k_R[d]
MBO231-RO_2	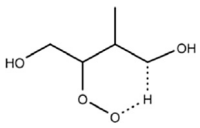	1,5-CH	18.1	10.8	1.3	7.3×10^{5}
MBO331-RO_2	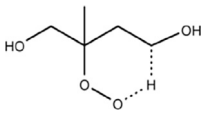	1,5-CH	18.4	12.1	1.6	1.3×10^{5}
MBO231-RO_2	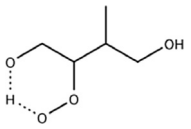	1,5-OH	22.3	2.3	4.8×10^{-4}	3.2×10^{11}
MBO331-RO_2	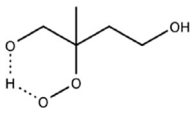	1,5-OH	22.7	3.4	3.3×10^{-4}	3.9×10^{10}
MBO232-RO_2	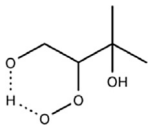	1,5a-OH	21.2	2.2	4.2×10^{-3}	1.8×10^{11}
MBO232-RO_2	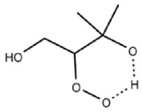	1,5b-OH	21.7	2.2	1.7×10^{-3}	3.0×10^{11}
MBO332-RO_2	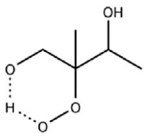	1,5a-OH	21.6	1.2	1.3×10^{-3}	5.7×10^{11}
MBO332-RO_2	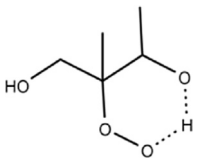	1,5b-OH	22.0	1.7	8.7×10^{-4}	4.1×10^{11}

[a] Zero-pointed corrected forward barrier ($RO_2 \rightarrow$ QOOH) in kcal mol^{-1}.
[b] Zero-pointed corrected reverse barrier (QOOH $\rightarrow RO_2$) in kcal mol^{-1}.
[c] Rate constant (k_{TST}) for the forward reaction ($RO_2 \rightarrow$ QOOH) in s^{-1}.
[d] Rate constant (k_{TST}) for the reverse reaction (QOOH $\rightarrow RO_2$) in s^{-1}.

and produce the products. Only around 8% of the MBO232-RO_2 will be thermalised in the MBO232-RO_2 energy well.

The ratios of the different reactions are dominated by the 1,5a-OH H-shift reaction and subsequent δ-scission, which produces 2-hydroxy-2-methyl-propanal (HmPR) and formaldehyde (CH_2O) with a ratio of 0.53. The second highest yield is from the 1,5b-OH H-shift reaction and subsequent β-scission, which produces acetone and glycolaldehyde with a ratio of 0.42. All other reactions are minor reactions.

3.3. Atmospheric impact of the H-shift reactions in the 2-methyl-3-buten-2-ol

From the MESMER simulation the three most important rate constants ($k_{Acet+Glyc}$, k_{14OO} and $k_{HmPR+CH2O}$) are implemented in the GEOS-Chem simulation. The implemented reactions are shown in the supplemental material. In our GEOS-Chem simulation the total MBO emission is 1.2 Tg yr^{-1}, which corresponds well with the previously estimated values (Guenther et al., 2012; Sindelarova et al., 2014). MBO232 is mainly emitted through summer and fall in the northern hemisphere (see Figure A.9 in the supplemental material). In Fig. 4 the annual average tropospheric column production (in molecules cm^{-2} s^{-1}) from each of the reactions are shown.

The reaction between MBO232-RO_2 and NO is the most important reaction (Fig. 4E), this means that acetone and glycolaldehyde are the main products from the atmospheric decomposition of MBO232. When the NO concentration is low (for example in the remote forest regions), the reaction of MBO232-RO_2 with HO_2 becomes important. The H-shift reactions are not able to compete with HO_2 reaction in these areas. The H-shift reactions are, therefore, of minor importance in the atmosphere (Fig. 4F versus

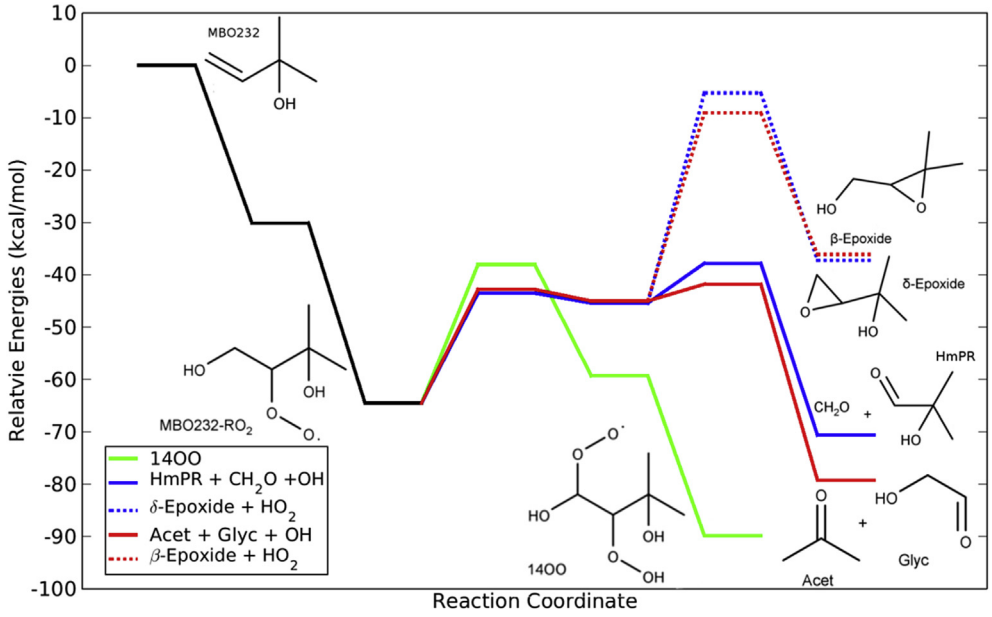

Fig. 3. The energy diagram for the atmospheric decomposition of MBO232 calculated with the M06-2X/aug-cc-pVTZ method. The black line is the energy profile of the OH radical addition to MBO232 and the subsequent reaction with O_2. All energies are relative to the energy of the MBO232 + OH + O_2. All the energies are zero-point corrected.

Table 2
The MESMER calculated overall rate constants (k_M) and product yields for the reaction MBO232-RO_2 → Products.

Reaction	Products	k_M (s^{-1})	Product yield in %
1,4-CH and $+O_2$	14OO	8.0×10^{-5}	5
1,5a-OH and α-scission	HmPR + CH_2O + OH	1.2×10^{-6}	53
1,5a-OH and epoxide	δ-Epoxide + HO_2	4.0×10^{-32}	N/a
1,5b-OH and β-scission	Acet + Glyc + OH	2.1×10^{-4}	42
1,5b-OH and epoxide	β-Epoxide + HO_2	5.1×10^{-29}	N/a

Fig. 4B–D). The yields for each of the reactions are shown in Table 3.

The major reaction of MBO232-RO_2 is the reaction with NO (85%) whereas the reaction with HO_2 (13%) or internal H-shift reactions (2%) are minor reactions. Our result are in good agreement with smog chamber experiments, where the main product in the oxidation of MBO232 is glycolaldehyde in both high and low NO_x experiments (Chan et al., 2009).

The products, acetone and glycolaldehyde, are formed when

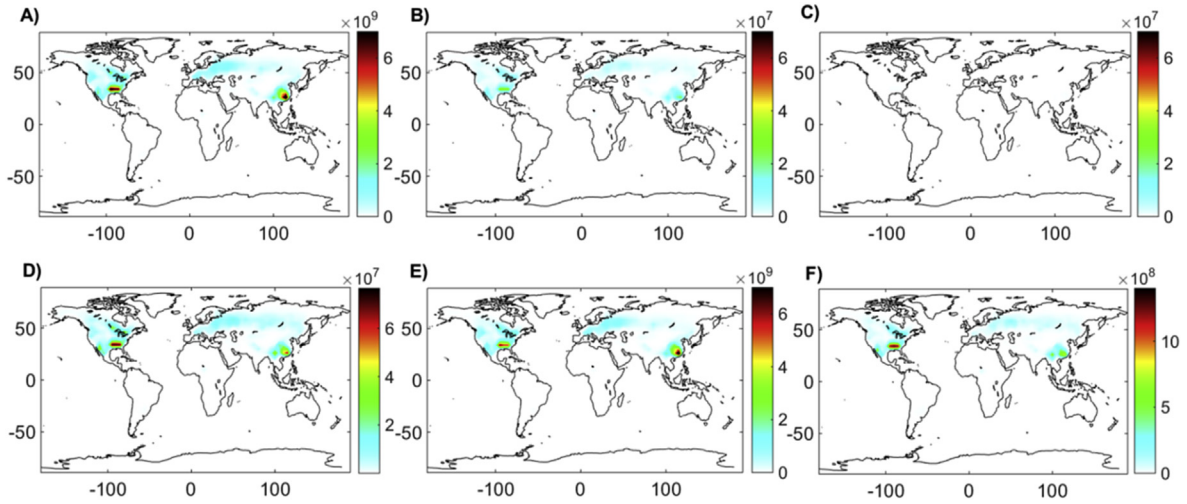

Fig. 4. The annual average tropospheric column production from each of the reactions in molecules cm^{-2} s^{-1}. The top left figure (Figure A) is the annual average total tropospheric column production summed for all of the reactions. The figures B–F are the annual average tropospheric column production for each of the reactions. Figure B) shows the production through the 1,4-CH H-shift reaction, the C) and D) are the production through the 1,5a-OH and 1,5b-OH H-shift reactions, respectively. Figure E) and F) are the annual average tropospheric column production from RO_2 reaction with either NO or HO_2, respectively. Figure B), C) and D) are scaled with a factor of 0.01 compared to Figure A), whereas Figure F) is scaled with a factor of 0.2 compared to Figure A).

Table 3
The reaction yield of each reaction channel in the atmospheric decomposition of MBO232-RO_2.

Products	Reaction yield in %
14OO	0.4
HmPR + CH_2O + OH	<0.1
Acet + Glyc + OH	1.1
Acet + Glyc + NO_2	85.2
ROOH	13.2

MBO232-RO_2 reacts with NO but they are also produced through the H-shift reactions. The total production through the H-shift reactions are about 9.1 and 9.4 Gg yr^{-1} of acetone and glycolaldehyde, respectively (see Table A.15 in the supplemental material). The total oxidation of MBO232 by the OH radical (through both the reaction with NO and the H-shift reaction) produces a total of about 0.7 Tg yr^{-1} of both acetone and glycolaldehyde. Acetone is a long-lived species in the atmosphere and is a significant source of HO_x radicals (Singh et al., 1995). The global emission of acetone is estimated to be around 43.7 Tg yr^{-1} (Guenther et al., 2012), hence the production of acetone from the OH radical oxidation of MBO232 is a minor atmospheric source on a global scale. Glycolaldehyde is known to oxidize into glyoxal (Bacher et al., 2001; Magneron et al., 2005). Glyoxal has been shown to be taken up by particles in the aqueous phase and hereby contribute to the secondary organic aerosol (SOA) particle growth in the atmosphere (Kroll et al., 2005; Liggio et al., 2005). Although the glycoaldehyde production through the H-shift reactions is low globally, the glycolaldehyde production could be important, where MBO232 emission is high and the concentrations of NO and HO_2 are low, see Fig. 4D.

4. Conclusion

We have investigated the H-shift reactions in four MBO peroxy radicals by calculating transition state theory rate constants with the M06-2X/aug-cc-pVTZ method. We observed that the 1,5-CH and 1,5-OH H-shift reactions are 10-10^4 times faster than the 1,4-CH and 1,6-OH H-shift reactions. The rate constants for the forward 1,5-CH H-shift reactions are about 1 s^{-1}, whereas the rate constants for the reverse reaction are about 10^5 s^{-1}. For the 1,5-OH H-shift reactions, the rate constants for the forward 1,5-OH H-shift are between 10^{-4}-10^{-3} s^{-1}, whereas the reverse H-shift reactions are very fast with rate constants around 10^{10}-10^{11} s^{-1}. We have further investigated the possible atmospheric impact of the H-shift reactions in MBO232. The GEOS-Chem simulation, showed that the H-shift reactions in the MBO232 peroxy radical are a minor atmospheric reaction with a total H-shift yield of about 2%, whereas the MBO232 peroxy radical reaction with NO was found to be 85% and 13% for the reaction with HO_2. Our results are in good agreement with earlier experimental findings and kinetically-inferred conclusions that the products from the MBO232 peroxy radicals predominantly comes from their reaction with NO or HO_2.

We investigated the possible H-shift reaction mechanism that could lead to the formation of gas-phase epoxides. We observed that the production of the epoxides was unlikely, since the barrier height for the epoxide formation is above 30 kcal/mol and hence the formation of the epoxide is very slow. We suggest that the possible SOA precursor potential of the 2-hydroperoxy-3-hydroxyisopentanol (ROOH) molecule are investigated in the future, since a substantial amount (13%) of ROOH is produced from MBO232-RO_2 reaction with HO_2 in the GEOS-Chem simulation.

Acknowledgment

We are grateful to Henrik G. Kjaergaard for helpful discussions. We would like to thank the Danish Council for Independent Research Natural Sciences and the Danish Center for Scientific Computing (DCSC) for funding. JAS acknowledge support from the Carlsberg Foundation.

Appendix A. Supplementary data

The supplementary material related to this article can be found at the Atmospheric Environment Publications website http://dx.doi.org/10.1016/j.atmosenv.2016.09.064.

References

Adler, T.B., Knizia, G., Werner, H.J., 2007. A simple and efficient CCSD(T)-F12 approximation. J. Chem. Phys. 127, 221106.
Alvarado, A., Tuazon, E.C., Aschmann, S.M., Arey, J., Atkinson, R., 1999. Products and mechanisms of the gas-phase reactions of OH radicals and O_3 with 2-methyl-3-buten-2-ol. Atmos. Environ. 33, 2893–2905.
Bacher, C., Tyndall, G.S., Orlando, J.J., 2001. The atmospheric chemistry of glycolaldehyde. J. Atmos. Chem. 39, 171–189.
Baker, B., Guenther, A., Greenberg, J., Goldstein, A., Fall, R., 1999. Canopy fluxes of 2-methyl-3-buten-2-ol over a ponderosa pine forest by relaxed eddy accumulation: field data and model comparison. J. Geophys. Res. 104, 26107–26114.
Becke, A.D., 1988. Density-functional exchange-energy approximation with correct asymptotic-behavior. Phys. Rev. A 38, 3098–3100.
Becke, A.D., 1993. Density-functional thermochemistry. 3. The role of exact exchange. J. Chem. Phys. 98, 5648–5652.
Bey, I., Jacob, D.J., Yantosca, R.M., Logan, J.A., Field, B.D., Fiore, A.M., Li, Q.B., Liu, H.G.Y., Mickley, L.J., Schultz, M.G., 2001. Global modeling of tropospheric chemistry with assimilated meteorology: model description and evaluation. J. Geophys. Res. 106, 23073–23095. www.geos-chem.org.
Boyd, A.A., Flaud, P.M., Daugey, N., Lesclaux, R., 2003. Rate constants for RO_2 + HO_2 reactions measured under a large excess of HO_2. J. Phys. Chem. A 107, 818–821.
Baasandorj, M., Stevens, P.S., 2007. Experimental and theoretical studies of the kinetics of the reactions of OH and OD with 2-methyl-3-buten-2-ol between 300 and 415 K at low pressure. J. Phys. Chem. A 111, 640–649.
Carrasco, N., Doussin, J.F., O'Connor, M., Wenger, J.C., Picquet-Varrault, B., Durand-Jolibois, R., Carlier, P., 2007. Simulation chamber studies of the atmospheric oxidation of 2-methyl-3-buten-2-ol: reaction with hydroxyl radicals and ozone under a variety of conditions. J. Atmos. Chem. 56, 33–55.
Chan, A.W.H., Galloway, M.M., Kwan, A.J., Chhabra, P.S., Keutsch, F.N., Wennberg, P.O., Flagan, R.C., Seinfeld, J.H., 2009. Photooxidation of 2-methyl-3-buten-2-ol (MBO) as a potential source of secondary organic aerosol. Environ. Sci. Technol. 43, 4647–4652.
Crounse, J.D., Knap, H.C., Ornso, K.B., Jørgensen, S., Paulot, F., Kjaergaard, H.G., Wennberg, P.O., 2012. Atmospheric fate of methacrolein. 1. Peroxy radical isomerization following addition of OH and O_2. J. Phys. Chem. A 116, 5756–5762.
Crounse, J.D., Nielsen, L.B., Jørgensen, S., Kjaergaard, H.G., Wennberg, P.O., 2013. Autoxidation of organic compounds in the atmosphere. J. Phys. Chem. Lett. 4, 3513–3520.
Crounse, J.D., Paulot, F., Kjaergaard, H.G., Wennberg, P.O., 2011. Peroxy radical isomerization in the oxidation of isoprene. Phys. Chem. Chem. Phys. 13, 13607–13613.
Cuadros, F., Cachadiña, I., Ahumada, W., 1996. Determination of Lennard-Jones interaction parameters using a new procedure. Mol. Eng. 6, 319–325.
Da Silva, G., Graham, C., Wang, Z.F., 2010. Unimolecular beta-hydroxyperoxy radical decomposition with OH recycling in the photochemical oxidation of isoprene. Environ. Sci. Technol. 44, 250–256.
Dunning, T.H., 1989. Gaussian-basis sets for use in correlated molecular calculations. 1. The atoms boron through neon and hydrogen. J. Chem. Phys. 90, 1007–1023.
Eckart, C., 1930. The penetration of a potential barrier by electrons. Phys. Rev. 35, 1303–1309.
Fantechi, G., Jensen, N.R., Hjorth, J., Peeters, J., 1998. Mechanistic studies of the atmospheric oxidation of methyl butenol by OH radicals, ozone and NO_3 radicals. Atmos. Environ. 32, 3547–3556.
Ferronato, C., Orlando, J.J., Tyndall, G.S., 1998. Rate and mechanism of the reactions of OH and Cl with 2-methyl-3-buten-2-ol. J. Geophys. Res. 103, 25579–25586.
Frisch, M.J., Pople, J.A., Binkley, J.S., 1984. Self-consistent molecular-orbital methods. 25. Supplementary functions for gaussian-basis sets. J. Chem. Phys. 80, 3265–3269.
Frisch, M.J., Trucks, G.W., Schlegel, H.B., Scuseria, G.E., Robb, M.A., Cheeseman, J.R., Scalmani, G., Barone, V., Mennucci, B., Petersson, G.A., et al., 2009. Gaussian 09, Revision B.1. Gaussian, Inc., Wallingford CT.
Glowacki, D.R., Liang, C.-H., Morley, C., Pilling, M.J., Robertson, S.H., 2012. MESMER: an open-source master equation solver for multi-energy well reactions. J. Phys. Chem. A 116, 9545–9560.

Goldan, P.D., Kuster, W.C., Fehsenfeld, F.C., Montzka, S.A., 1993. The observation of a C_5 alcohol emission in a North-American pine forest. Geophys. Res. Lett. 20, 1039–1042.
Gonzalez, C., Schlegel, H.B., 1989. An improved algorithm for reaction-path following. J. Chem. Phys. 90, 2154–2161.
Gonzalez, C., Schlegel, H.B., 1990. Reaction-path following in mass-weighted internal coordinates. J. Phys. Chem. 94, 5523–5527.
Guenther, A.B., Jiang, X., Heald, C.L., Sakulyanontvittaya, T., Duhl, T., Emmons, L.K., Wang, X., 2012. The model of emissions of gases and aerosols from nature version 2.1 (MEGAN2.1): an extended and updated framework for modeling biogenic emissions. Geosci. Model Dev. 5, 1471–1492.
Harley, P., Fridd-Stroud, V., Greenberg, J., Guenther, A., Vasconcellos, P., 1998. Emission of 2-methyl-3-buten-2-ol by pines: a potentially large natural source of reactive carbon to the atmosphere. J. Geophys. Res. 103, 25479–25486.
Holbrook, K.A., Pilling, M.J., Robertson, S.H., 1996. Unimolecular Reactions, second ed. Wiley.
Jaoui, M., Kleindienst, T.E., Offenberg, J.H., Lewandowski, M., Lonneman, W.A., 2012. SOA formation from the atmospheric oxidation of 2-methyl-3-buten-2-ol and its implications for PM2.5. Atmos. Chem. Phys. 12, 2173–2188.
Jørgensen, S., Knap, H.C., Otkær, R.V., Jensen, A.M., Kjeldsen, M.L.H., Wennberg, P.O., Kjaergaard, H.G., 2016. Rapid hydrogen shift scrambling in hydroperoxy substituted organic peroxy radicals. J. Phys. Chem. A 120, 266–275.
Knap, H.C., Jørgensen, S., Kjaergaard, H.G., 2015. Theoretical investigation of the hydrogen shift reactions in peroxy radicals derived from the atmospheric decomposition of 3-methyl-3-buten-1-ol (MBO331). Chem. Phys. Lett. 619, 236–240.
Koenig, G., Brunda, M., Puxbaum, H., Hewitt, C.N., Duckham, S.C., Rudolph, J., 1995. Relative contribution of oxygenated hydrocarbons to the total biogenic VOC emissions of selected mid-European agricultural and natural plant species. Atmos. Environ. 29, 861–874.
Kroll, J.H., Ng, N.L., Murphy, S.M., Varutbangkul, V., Flagan, R.C., Seinfeld, J.H., 2005. Chamber studies of secondary organic aerosol growth by reactive uptake of simple carbonyl compounds. J. Geophys. Res. 110, D23207.
Lane, J.R., Kjaergaard, H.G., 2009. Explicitly correlated intermolecular distances and interaction energies of hydrogen bonded complexes. J. Chem. Phys. 131, 034307.
Lee, C.T., Yang, W.T., Parr, R.G., 1988. Development of the Colle-Salvetti correlation-energy formula into a function of the electron-density. Phys. Rev. B 37, 785–789.
Liggio, J., Li, S.M., McLaren, R., 2005. Reactive uptake of glyoxal by particulate matter. J. Geophys. Res. 110, D10304.
Magneron, I., Mellouki, A., Le Bras, G., Moortgat, G.K., Horowitz, A., Wirtz, K., 2005. Photolysis and OH-initiated oxidation of glycolaldehyde under atmospheric conditions. J. Phys. Chem. A 109, 4552–4561.
Marchetti, O., Werner, H.J., 2009. Accurate calculations of intermolecular interaction energies using explicitly correlated coupled cluster wave functions and a dispersion-weighted MP2 method. J. Phys. Chem. A 113, 11580–11585.
Orlando, J.J., Tyndall, G.S., 2012. Laboratory studies of organic peroxy radical chemistry: an overview with emphasis on recent issues of atmospheric significance. Chem. Soc. Rev. 41, 6294–6317.
Park, J., Jongsma, C.G., Zhang, R.Y., North, S.W., 2004. OH/OD initiated oxidation of isoprene in the presence of O_2 and NO. J. Phys. Chem. A 108, 10688–10697.
Paulot, F., Crounse, J.D., Kjaergaard, H.G., Kurten, A., St Clair, J.M., Seinfeld, J.H., Wennberg, P.O., 2009. Unexpected epoxide formation in the gas-phase photooxidation of isoprene. Science 325, 730–733.
Peeters, J., Muller, J.F., Stavrakou, T., Nguyen, V.S., 2014. Hydroxyl radical recycling in isoprene oxidation driven by hydrogen bonding and hydrogen tunneling: the upgraded LIM1 mechanism. J. Phys. Chem. A 118, 8625–8643.
Peeters, J., Nguyen, T.L., 2012. Unusually fast 1,6-H shifts of enolic hydrogens in peroxy radicals: formation of the first-generation C_2 and C_3 carbonyls in the oxidation of isoprene. J. Phys. Chem. A 116, 6134–6141.
Peeters, J., Nguyen, T.L., Vereecken, L., 2009. HOx radical regeneration in the oxidation of isoprene. Phys. Chem. Chem. Phys. 11, 5935–5939.
Peterson, K.A., Adler, T.B., Werner, H.J., 2008. Systematically convergent basis sets for explicitly correlated wavefunctions: the atoms H, He, B-Ne, and Al-Ar. J. Chem. Phys. 128, 084102.
Reisen, F., Aschmann, S.M., Atkinson, R., Arey, J., 2003. Hydroxyaldehyde products from hydroxyl radical reactions of Z-3-hexen-1-ol and 2-methyl-3-buten-2-ol quantified by SPME and API-MS. Environ. Sci. Technol. 37, 4664–4671.
Rissanen, M.P., Kurten, T., Sipila, M., Thornton, J.A., Kangasluoma, J., Sarnela, N., Junninen, H., Jørgensen, S., Schallhart, S., Kajos, M.K., et al., 2014. The formation of highly oxidized multifunctional products in the ozonolysis of cyclohexene. J. Am. Chem. Soc. 136, 15596–15606.
Sindelarova, K., Granier, C., Bouarar, I., Guenther, A., Tilmes, S., Stavrakou, T., Muller, J.F., Kuhn, U., Stefani, P., Knorr, W., 2014. Global data set of biogenic VOC emissions calculated by the MEGAN model over the last 30 years. Atmos. Chem. Phys. 14, 9317–9341.
Singh, H.B., Kanakidou, M., Crutzen, P.J., Jacob, D.J., 1995. High concentrations and photochemical fate of oxygenated hydrocarbons in the global troposphere. Nature 378, 50–54.
Spartan'10, 2010. Wavefunction Inc., Irivine CA.
St Clair, J.M., Rivera-Rios, J.C., Crounse, J.D., Knap, H.C., Bates, K.H., Teng, A.P., Jørgensen, S., Kjaergaard, H.G., Keutsch, F.N., Wennberg, P.O., 2016. Kinetics and products of the reaction of the first-generation isoprene hydroxy hydroperoxide (ISOPOOH) with OH. J. Phys. Chem. A 120, 1441–1451.
Vereecken, L., Nguyen, T.L., Hermans, I., Peeters, J., 2004. Computational study of the stability of alpha-hydroperoxyl-alpha-alkylperoxyl substituted alkyl radicals. Chem. Phys. Lett. 393, 432–436.
Werner, H.-J., Knowles, P.J., Knizia, G., Manby, F.R., Schütz, M., Celani, P., Korona, T., Lindh, R., Mitrushenkov, A., Rauhut, G., et al., 2012a. MOLPRO, Version 2012.1 a package of ab initio programs. http://www.molpro.net.
Werner, H.J., Knowles, P.J., Knizia, G., Manby, F.R., Schutz, M., 2012b. Molpro: a general-purpose quantum chemistry program package. Wiley Interdiscip. Reviews-Comput. Mol. Sci. 2, 242–253.
Zhang, F., Dibble, T.S., 2011. Impact of tunneling on hydrogen-migration of the n-propylperoxy radical. Phys. Chem. Chem. Phys. 13, 17969–17977.
Zhang, H., Worton, D.R., Lewandowski, M., Ortega, J., Rubitschun, C.L., Park, J.-H., Kristensen, K., Campuzano-Jost, P., Day, D.A., Jimenez, J.L., et al., 2012. Organosulfates as tracers for secondary organic aerosol (SOA) formation from 2-methyl-3-buten-2-ol (MBO) in the atmosphere. Environ. Sci. Technol. 46, 9437–9446.
Zhang, H., Zhang, Z., Cui, T., Lin, Y.-H., Bhathela, N.A., Ortega, J., Worton, D.R., Goldstein, A.H., Guenther, A., Jimenez, J.L., et al., 2014. Secondary organic aerosol formation via 2-methyl-3-buten-2-ol photooxidation: evidence of acid-catalyzed reactive Uptake of epoxides. Environ. Sci. Technol. Lett. 1, 242–247.
Zhao, Y., Truhlar, D.G., 2008. The M06 suite of density functionals for main group thermochemistry, thermochemical kinetics, noncovalent interactions, excited states, and transition elements: two new functionals and systematic testing of four M06-class functionals and 12 other functionals. Theor. Chem. Acc. 120, 215–241.